Search for diffuse neutrino flux from astrophysical sources with MACRO

MACRO Collaboration

M. Ambrosio [a], R. Antolini [b], G. Auriemma [c,d], D. Bakari [e,f], A. Baldini [g],
G.C. Barbarino [a], B.C. Barish [h], G. Battistoni [i,j], Y. Becherini [e], R. Bellotti [k],
C. Bemporad [g], P. Bernardini [l], H. Bilokon [i], C. Bloise [i], C. Bower [m],
M. Brigida [k], S. Bussino [n], F. Cafagna [k], M. Calicchio [k], D. Campana [a],
M. Carboni [i], R. Caruso [o], S. Cecchini [e,p], F. Cei [g], V. Chiarella [i],
B.C. Choudhary [h], S. Coutu [q,r], M. Cozzi [e], G. De Cataldo [k], H. Dekhissi [e,f],
C. De Marzo [k], I. De Mitri [l], J. Derkaoui [e,f], M. De Vincenzi [n], A. Di Credico [b],
O. Erriquez [k], C. Favuzzi [k], C. Forti [i], P. Fusco [k], G. Giacomelli [e], G. Giannini [g,s],
N. Giglietto [k], M. Giorgini [e], M. Grassi [g], A. Grillo [b], F. Guarino [a],
C. Gustavino [b], A. Habig [t,u], K. Hanson [q], R. Heinz [m], E. Iarocci [i,v],
E. Katsavounidis [h,w], I. Katsavounidis [h,x], E. Kearns [t], H. Kim [h],
S. Kyriazopoulou [h], E. Lamanna [c,y], C. Lane [z], D.S. Levin [q], P. Lipari [c],
N.P. Longley [h,aa], M.J. Longo [q], F. Loparco [k], F. Maaroufi [e,f], G. Mancarella [l],
G. Mandrioli [e], A. Margiotta [e], A. Marini [i], D. Martello [l], A. Marzari-Chiesa [ab],
M.N. Mazziotta [k], D.G. Michael [h], P. Monacelli [o], T. Montaruli [k],
M. Monteno [ab], S. Mufson [m], J. Musser [m], D. Nicolò [g], R. Nolty [h], C. Orth [t],
G. Osteria [a], O. Palamara [b], V. Patera [i,v], L. Patrizii [e], R. Pazzi [g], C.W. Peck [h],
L. Perrone [l,*], S. Petrera [o], P. Pistilli [n], V. Popa [e,ac], A. Rainò [k], J. Reynoldson [b],
F. Ronga [i], A. Rrhioua [e,f], C. Satriano [c,d], E. Scapparone [b], K. Scholberg [t,w],
A. Sciubba [i,v], P. Serra [e], M. Sioli [e], G. Sirri [e], M. Sitta [ab,ad], P. Spinelli [k],
M. Spinetti [i], M. Spurio [e], R. Steinberg [z], J.L. Stone [t], L.R. Sulak [t], A. Surdo [l],
G. Tarlè [q], V. Togo [e], M. Vakili [ae,af], C.W. Walter [t], R. Webb [ae]

[a] *Dipartimento di Fisica dell'Università di Napoli and INFN, 80125 Napoli, Italy*
[b] *Laboratori Nazionali del Gran Sasso dell'INFN, 67010 Assergi (L'Aquila), Italy*
[c] *Dipartimento di Fisica dell'Università di Roma "La Sapienza" and INFN, 00185 Roma, Italy*
[d] *Università della Basilicata, 85100 Potenza, Italy*

---

* Corresponding author. Tel.: +39-832-320-459; fax: +39-832-320-505.
E-mail address: lorenzo.perrone@le.infn.it (L. Perrone).

[e] *Dipartimento di Fisica dell'Università di Bologna and INFN, 40126 Bologna, Italy*

[f] *L.P.T.P, Faculty of Sciences, University Mohamed I, B.P. 524 Oujda, Morocco*

[g] *Dipartimento di Fisica dell'Università di Pisa and INFN, 56010 Pisa, Italy*

[h] *California Institute of Technology, Pasadena, CA 91125, USA*

[i] *Laboratori Nazionali di Frascati dell'INFN, 00044 Frascati (Roma), Italy*

[j] *INFN Milano, 20133 Milano, Italy*

[k] *Dipartimento di Fisica dell'Università di Bari and INFN, 70126 Bari, Italy*

[l] *Dipartimento di Fisica dell'Università di Lecce and INFN, Sezione di Lecce Via Arnesano CP 193, 73100 Lecce, Italy*

[m] *Department of Physics and of Astronomy, Indiana University, Bloomington, IN 47405, USA*

[n] *Dipartimento di Fisica dell'Università di Roma Tre and INFN Sezione Roma Tre, 00146 Roma, Italy*

[o] *Dipartimento di Fisica dell'Università dell'Aquila and INFN, 67100 L'Aquila, Italy*

[p] *Istituto IASF/CNR, 40129 Bologna, Italy*

[q] *Department of Physics, University of Michigan, Ann Arbor, MI 48109, USA*

[r] *Department of Physics, Pennsylvania State University, University Park, PA 16801, USA*

[s] *Università di Trieste and INFN, 34100 Trieste, Italy*

[t] *Physics Department, Boston University, Boston, MA 02215, USA*

[u] *Duluth Physics Department, University of Minnesota, Duluth, MN 55812, USA*

[v] *Dipartimento di Energetica, Università di Roma, 00185 Roma, Italy*

[w] *Department of Physics, MIT, Cambridge, MA 02139, USA*

[x] *Intervideo Inc., Torrance CA 90505, USA*

[y] *Dipartimento di Fisica dell'Università della Calabria, 87036 Rende (Cosenza), Italy*

[z] *Department of Physics, Drexel University, Philadelphia, PA 19104, USA*

[aa] *Department of Physics and Astronomy, Macalester College, St. Paul, MN 55105, USA*

[ab] *Dipartimento di Fisica Sperimentale dell'Università di Torino and INFN, 10125 Torino, Italy*

[ac] *Institute for Space Sciences, 76900 Bucharest, Romania*

[ad] *Dipartimento di Scienze e Tecnologie Avanzate, Università del Piemonte Orientale, 15100 Alessandria, Italy*

[ae] *Physics Department, Texas A&M University, College Station, TX 77843, USA*

[af] *Resonance Photonics, Markham, Ont., L3R 5B1, Canada*

Abstract

Many galactic and extragalactic astrophysical sources are currently considered promising candidates as high-energy neutrino emitters. Astrophysical neutrinos can be detected as upward-going muons produced in charged-current interactions with the medium surrounding the detector. The expected neutrino fluxes from various models start to dominate on the atmospheric neutrino background at neutrino energies above some tens of TeV. We present the results of a search for an excess of high-energy upward-going muons among the sample of data collected by MACRO during $\sim$5.8 years of effective running time. No significant evidence for this signal was found. As a consequence, an upper limit on the flux of upward-going muons from high-energy neutrinos was set at the level of 1.7×10^{-14} cm^{-2} s^{-1} sr^{-1}. The corresponding upper limit for the diffuse neutrino flux was evaluated assuming a neutrino power law spectrum. Our result was compared with theoretical predictions and upper limits from other experiments.
© 2002 Elsevier Science B.V. All rights reserved.

1. Neutrino astronomy: overview and motivation

Neutrinos with energies larger than $\sim$1 GeV are expected from a wide class of galactic and extra-galactic astrophysical sources. Neutrino production requires the existence of hadronic processes and it is generally described in the picture of the *beam dump model* [1]: high-energy protons

accelerated close to compact objects by shock waves or plasma turbulence interact with photons or target matter surrounding the source, producing pions. Neutrinos of electron and muon flavors originate from decays of charged pions, as well from subsequent muon decays. In the same hadronic chains, high-energy γ-rays are expected to be produced through neutral pion decays. Like γ-rays, neutrinos can travel undeflected through the Universe. Neutrinos however are much less absorbed than photons and thus make a more powerful *probe* for astronomy searches. Many of the candidate sources of neutrinos (binary systems, supernovae remnants, AGNs, GRBs, etc) have already been recognized as gamma rays emitters at energies higher than 1 TeV: this provides an important hint for neutrino astronomy, even though the observed γ-ray energies are not high enough to exclude the electromagnetic production mechanisms, such as synchrotron or inverse Compton processes. In this scenario, the detection of high-energy neutrinos would open a new field of research, complementary to γ-ray astronomy.

Neutrinos coming from a source propagate through the Earth, occasionally producing upward-going muons by charged-current interactions with the matter surrounding the detector. The detection probability grows with the energy due to the increase of both neutrino–nucleon cross sections and muon range, so that the effective detector mass results from the convolution of the detector area with the muon path-length.

Underwater/ice neutrino detectors like Baikal [2] and AMANDA [3], as well as underground experiments like MACRO [4], IMB [5], Baksan [6] and Superkamiokande [7], surveyed the sky in order to search for point source of astrophysical neutrinos. At the present their effective area is not large enough to measure the expected flux but they set experimental upper limits that guide and constrain theoretical models. Next generation neutrino telescopes like ANTARES [8], Icecube [9], NEMO [10] and NESTOR [11], with effective areas ranging from 0.1 to 1 km^2, are expected to provide the sensitivity required for observing astrophysical sources. A detailed review dealing with physics goals and detection techniques in the field of neutrino astronomy can be found in [12].

The results of a search for point-like sources was recently presented by the MACRO Collaboration in [4]. Here we show the results of a search for a diffuse neutrino flux from unresolved sources, by looking for an excess of high-energy upward-going events. A preliminary study of the sensitivity of the MACRO detector to high-energy muons is in [13]. In Section 2 we discuss the capability of the MACRO detector as a neutrino telescope. In particular, since most of events induced by astrophysical neutrinos are expected in the 0.1–100 TeV energy range, the response of scintillation counters was accurately studied for high-energy events, using the scintillator calibrations. In Section 3 we show that the energy released in the scintillation counters by crossing muons is the most important information for the selection of events induced by astrophysical neutrinos. We describe the analysis cuts on the events from a simulated signal, and in Section 4 on the events from the expected background. The main background source are upward-going muons induced from atmospheric neutrinos. The GEANT-based [14] simulation tool used by MACRO [15] was modified to correctly handling the propagation of very high-energy (VHE) muons in the rock surrounding the detector [16], and the detector response for events with high-energy releases. In Section 5 we present the results of the analysis of the real data sample, and we give the upper limit for the diffuse neutrino flux from unresolved sources. This upper limit is compared with some theoretical predictions and with upper limits from other experiments.

2. MACRO as a neutrino telescope

MACRO, located at the Gran Sasso Laboratories (Italy), was a large area multipurpose underground detector, in the shape of a rectangular box whose global dimensions were $76.6 \times 12.0 \times 9.3$ m^3 [15]. The lower half of the apparatus was filled with rock absorber alternating with streamer tube planes for particle tracking. Liquid scintillator layers, placed at the bottom, the center, the top and all around the detector provided time information for discriminating the direction of incoming particles. The horizontal streamer tube planes

were equipped with pick-up strips providing stereo readout of the detector hits. The large acceptance ($\sim 10^4$ m^2 sr for an isotropic flux), the good shielding of the site (the rate of cosmic ray muons is $\sim 10^{-6}$ times the surface rate), the fast timing (time resolution ~ 0.5 ns) and the good pointing capability (intrinsic angular resolution $\lesssim 1°$) made MACRO suitable for working as a neutrino *telescope*.

2.1. Scintillator response and photomultiplier saturation

The energy deposited in a MACRO scintillation counter by a throughgoing particle is reconstructed by the Energy Reconstruction Processor (ERP) system according to the procedure described in [15].

The ERP circuit uses a twelve-bit ADC that makes an accurate integration of the photomultiplier pulse. This is applied to both the raw signal and a $10\times$ attenuated version; the latter was used when the non-attenuated ADC saturates, i.e. for fast magnetic monopole searches [17] and in this analysis. The ERP provides also time of flight from two TDCs readout. The ERP ADCs and TDCs were calibrated weekly with delayed LED signals and variable-intensity laser pulses. The ADCs energy calibrations assume a linear relationship between the number of attenuated ADC counts and the light hitting the phototube L:

$$L = G(\mathrm{ADC} - p) \tag{1}$$

where G and p are the gain factor and the pedestal of each scintillation counter, respectively. This hypothesis is valid for most of the analyses based on MACRO data.

The present analysis deals with signals greatly exceeding the average energy released in the detector by downward-going cosmic ray muons and atmospheric neutrino-induced events. If the energy released in a counter exceeds 4–5 times the level of that released by minimum ionizing cosmic ray muons ($\simeq 34$ MeV for one vertical track crossing a horizontal scintillation counter), the phototube response is not linear anymore [17]. The effect of photomultiplier saturation can be taken into account by including in Eq. (1) the next-to-leading

order terms. By following the approach described in [17], Eq. (1) becomes:

$$L = G(\mathrm{ADC} - p) + \mathscr{D}(\mathrm{ADC} - p)^2 \\ + \mathscr{T}(\mathrm{ADC} - p)^3 + \mathscr{F}(\mathrm{ADC} - p)^4 \tag{2}$$

the constants $\mathscr{D}$, $\mathscr{T}$, $\mathscr{F}$ represent the second-, the third-, and the fourth-order corrections. These parameters were determined (one set for each MACRO scintillation counter) by fitting the laser light yield L versus the ERP ($\mathrm{ADC} - p$) value with a fourth degree polynomial. G and p are fixed at the value given by the standard ERP energy calibration.

In Fig. 1 (upper panel), the linear and the non-linear response regions are shown for one of the horizontal counters. The empty circles represent the mean values of the gaussian distributed ADC response for a fixed light level. The dashed curve shows the fourth-order fit done by taking into account the statistical errors. The standard energy reconstruction is reliable below few times the minimum ionizing particle (MIP) level. This analysis searches for events with a large energy release, above a certain threshold. For this reason, we used the correction given in Eq. (2), which makes the energy reconstruction reliable above 3 MIP and up to ~ 15 MIP (i.e. ~ 500 MeV in a single counter). Above this value, the energy reconstruction may be affected by a large error because of the saturation. The fit constants $\mathscr{D}$, $\mathscr{T}$, $\mathscr{F}$ and the parameters G and p of Eq. (2) were supposed independent on the time. This approximation is verified within 10% accuracy for the constants G and p measured with the standard calibration procedures. For the purpose of our analysis, a reconstructed energy $\geqslant 500$ MeV will be considered as an indication of a large energy release.

The lower panel of Fig. 1 shows the distribution of the total energy released in the scintillators by a sample of 80,000 real events collected by MACRO (downward-going cosmic ray muons). In particular, the solid line is obtained using Eq. (2), whereas the dashed line is obtained using the standard calibrations (Eq. (1)). The corrections act only at large values of released energy E_{Rel}, while around the distribution maximum their effect is negligible. Ignoring the photomultiplier non-linearity leads to
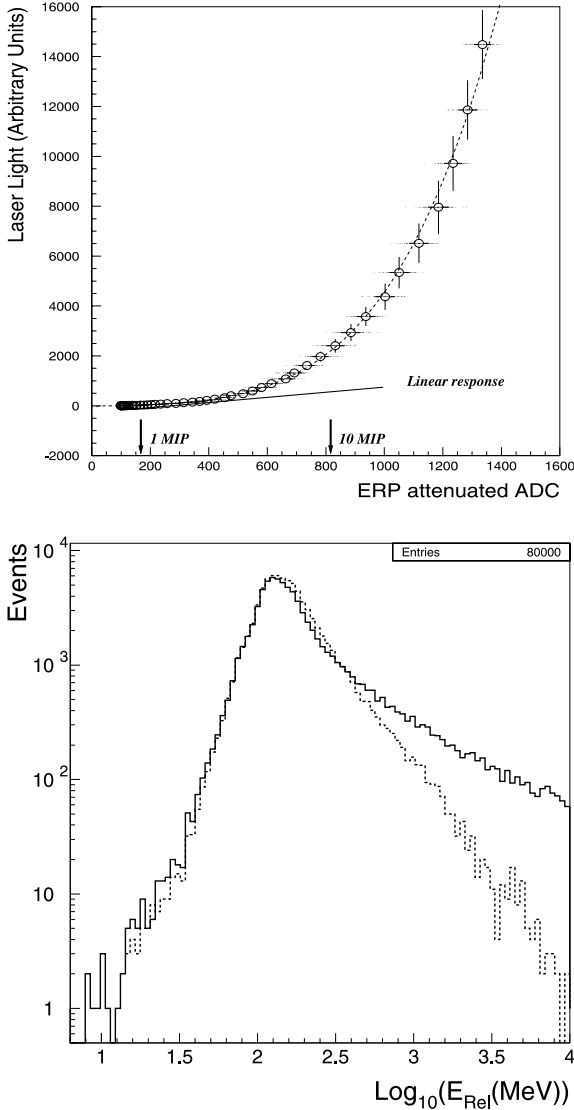
Fig. 1. (Upper) ERP attenuated ADC response to laser light with linear and fourth-order fits. The plot is for one of the horizontal counters. The single (1 MIP) and ten-times (10 MIP) minimum ionizing particle levels are shown (for a vertical track crossing the center of the counter). (Lower) Distribution of the total released energy E_{Rel} for a sample of 80,000 downward-going muons in MACRO; (- - -) E_{Rel} calculated with the linear response Eq. (1); (—) E_{Rel} calculated with Eq. (2).

a systematic underestimate of the reconstructed energy loss for a small fraction of high-energy events. This is in agreement with what it is ex-

pected from the curve given on the upper panel of Fig. 1 in the saturation region: a fixed ADC value corresponds to a value of the reconstructed energy higher than in the case of the linear response approximation.

3. Monte Carlo simulation of the AGN signal

This analysis aims to select a sample of VHE upward-going muons, since at neutrino energies above some tens of TeV the predicted neutrino fluxes from astrophysical sources start to rise above the atmospheric neutrino background. In our simulation of the AGN signal in MACRO we used as input the model by Stecker et al. [18] for the photopion production of neutrinos in AGN core.

Because high-energy neutrino absorption from the Earth is an important effect, the neutrino propagation through the Earth was done by solving the kinetic equation for the transport of neutrinos in dense media. This approach is suggested in [19], where the neutrino absorption and the contribution of neutrino–nucleon neutral-current interactions were properly taken into account. The deep inelastic cross sections were calculated using the set of parton density functions CTEQ3-DIS [20]. The new version of parton density functions by CTEQ group [21] does not produce significant changes for our calculation. The neutrino-induced muon propagation in the rock outside the detector was evaluated using the analytical formulas given in [16,22].

Then, following the analytical distributions, we simulated a sample of 13305 upward-going muons on the surface of a volume containing the detector plus 2-m-wide layer of surrounding rock. The rock was included to take into account the effect of electromagnetic showers induced by the muons in the detector. In this volume, the transport of muons was done with the tool developed in [16], which correctly propagate VHE muons up to the PeV energies. This software package replaced in our simulation the default transport modules implemented in the GEANT [14] package.

By normalizing to the expected event rate from the model by Stecker et al. (4.45 events/year on the

surface of this box) our simulated sample is equivalent to $T_{eq} = 2988.5$ years. 7547/13305 simulated muons reach the active detector and hit at least one scintillation counter in two different layers of the MACRO detector. This was the minimum requirement to define an "event".

We adopt the following notation: taking as a reference the upper counter which measures the time T_1, the time of flight $\Delta T = T_2 - T_1$ is positive if the particle travels downward and it is negative if the particle travels upwards. Two or more adjacent scintillator hits within a time window of 2 ns and on the same detector layer, at a maximum distance of 1 m, form a *scintillator cluster*. Any association between a cluster and a single hit placed on different layers, as well as between two different clusters on different layers defines a *scintillator track*. The scintillator track length is the geometrical distance between the positions of the center of each cluster. If a *cluster* contains more than one counter, its center is calculated by averaging the hit positions weighted with the released energy. For each scintillator track, the quantity $1/\beta = c\Delta T/L$ (L is the track length and c the speed of light) in our convention is around $+1$ for

downward-going particles and -1 in the opposite case.

Fig. 2 (left) shows the correlation between the reconstructed total energy released in the scintillator E_{Rel}, with the muon initial energy $E_{Initial}$. By initial energy we mean the energy of the muons when they enter the detector. Each simulated event is represented with a point in the scatter plot.

In order to reduce the background due to atmospheric neutrino-induced muons (see next section), we select the VHE muons from the AGN simulated signal by imposing more and more stringent conditions, the effects of which are illustrated in Fig. 2 (right). The light shaded histogram corresponds to events for which there is at least one scintillator with energy release greater than 500 MeV; the histogram with the dark shaded area corresponds to events with at least two scintillators, each one with energy release greater than 500 MeV, and distance between the hits smaller than 1 m; the histogram with the black shaded area corresponds to events with a further scintillator in a different detector layer and with energy release greater than 500 MeV. The darker points on Fig. 2 (left) represent the subsample of events, which
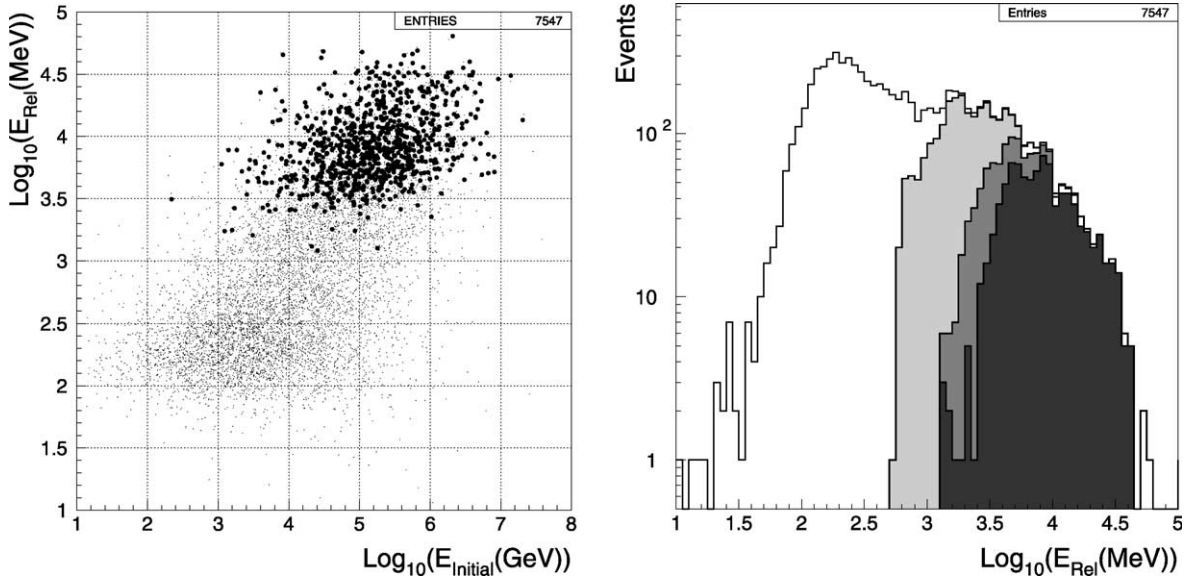

Fig. 2. (Left) Scatter plot of the reconstructed total energy E_{Rel} released in the scintillator counters versus the muon initial energy $E_{Initial}$. Each simulated event is represented with a point. The darker points represent the subsample of events which survived all the cuts described in the text. (Right) The effect of more and more stringent cuts (see text) on E_{Rel} to select the subsample of high-energy muons.

survived all the cuts described above. Hereafter we will refer to the last condition as E_{cut}. In Fig. 2 (right) the principal maximum of the light shaded distribution is due to the muons which lose energy through standard ionization. The second "bump" is populated by higher energy muons, with large energy release in the scintillators through radiative processes. The value of $E_{Rel} = 500$ MeV was chosen after the calibration procedure described in Section 2.

To discriminate the direction of the incoming events an algorithm based on the time-of-flight technique was developed. The algorithm calculates the mean time associated with each scintillator layer involved in the event. We required a reconstructed upward-going flight direction between at least two different scintillator layers. This condition for selecting upward-going events was called $D1_{cut}$.

Many scintillator tracks (associations between any two *scintillator clusters*) are present in a showering event. Thus, a more selective cut for discriminating the upward direction, can be imposed using all the scintillator tracks in the event. We required that the ratio between the number of tracks with positive $1/\beta$ value (downward-going) and negative $1/\beta$ (upward-going) is less than 0.4 (cut $D2_{cut}$). The value of the ratio was optimized using a Monte Carlo study on a simulated sample of $\sim 10^6$ downward-going muons: no downward-going muons survived the energy cut E_{cut} combined with the direction cut D_{cut}, defined as $D1_{cut} + D2_{cut}$. After the cuts $E_{cut} + D_{cut}$, 438/13305 simulated VHE neutrino-induced muons (signal) survived.

Fig. 3 shows the distribution of the simulated cosine of muon zenith angle θ_{sim}. The solid histogram refers to the overall sample of simulated events; the dashed histogram represents the sample selected after the $E_{cut} + D_{cut}$. The $\cos\theta_{sim}$ dependence of the muon flux is a consequence of high-energy neutrino absorption of the Earth [23]. Even assuming an isotropic neutrino flux [18] as input model, the zenith angular distribution of muons reaching the detector shows a strong suppression at $\cos\theta_{sim} \leqslant -0.8$ due to the hard discontinuity of the Earth density profile in correspondence of the massive nucleus.
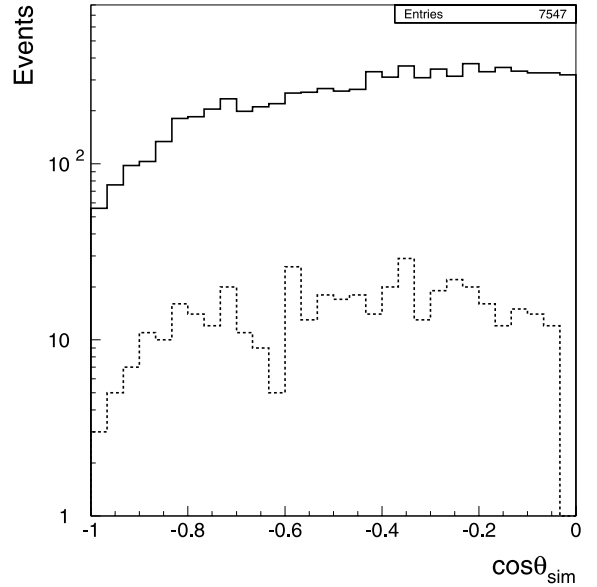

Fig. 3. Distribution of the cosine of zenith angle for the overall sample of simulated events (—). The dashed histogram refers to the events selected by the energy cut E_{cut} combined with the direction cut D_{cut}.

Fig. 4 shows the selection efficiency of the analysis cuts $E_{cut} + D_{cut}$, when applied to the simulated sample of events from AGNs. In the left plot such efficiency is shown as a function of the cosine of muon zenith angle θ_{zen}, while the right one represents the dependence on the muon initial energy.

The energy cut E_{cut} and the flight direction cut D_{cut} were not completely efficient to reject atmospheric multiple muons and nearly horizontal high-energy cosmic ray muons. These events generate large showers in the apparatus, with a large number of scintillator tracks. Thus, a final cut was defined in order to improve the capability of selecting upward-going events against the background of downward-going showering events. For each event, we define as: *itot*, the number of scintillator tracks whose length is greater than 2.5 m; *iup*, the number of scintillator tracks for which $-1.25 \leqslant 1/\beta \leqslant -0.75$; *idown*, the number of scintillator tracks for which $0.75 \leqslant 1/\beta \leqslant 1.25$. The final cut (called S_{cut}: itot > 11 and iup/itot > 0.3 and idown/iup < 0.1) selects upward-going events for events with a large number of scintillator
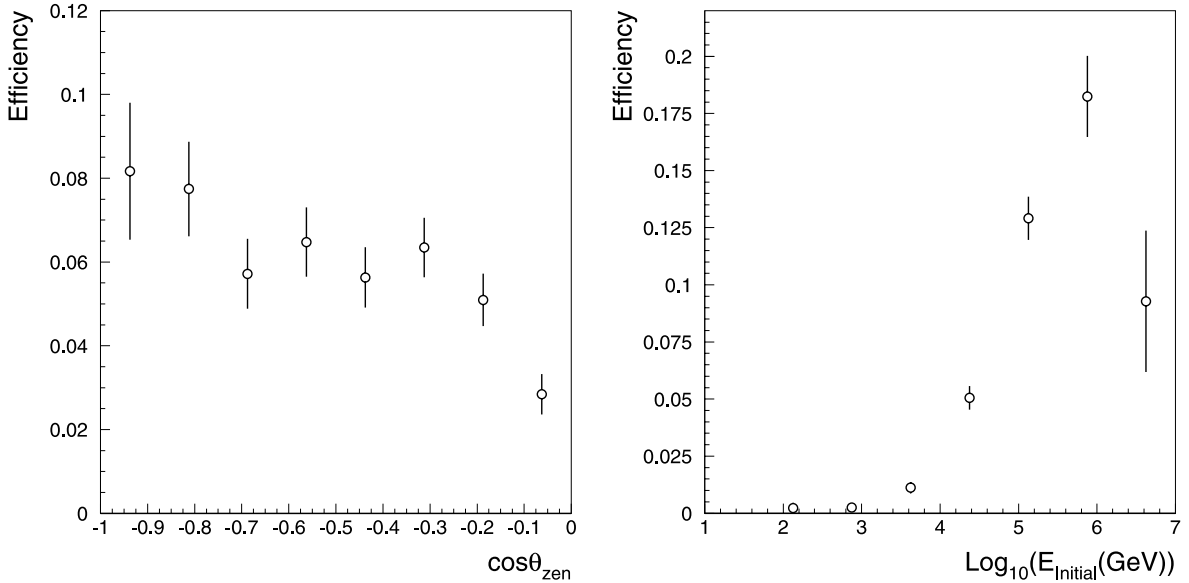
Fig. 4. Efficiency of analysis cuts $E_{\text{cut}} + D_{\text{cut}}$ for selecting muons from the simulated AGN signal, as a function of the muon zenith angle (left) and of the muon initial energy (right). Only the statistical errors due to the limited simulation sample are shown.

tracks. This cut was tuned to reject Monte Carlo simulated background events and the large sample of multiple muons and nearly horizontal high-energy cosmic ray muons in the real data. After this last cut, 247/13305 simulated VHE signal events survived.

4. The background of atmospheric neutrinos

The background from atmospheric neutrinos was estimated with the Monte Carlo program developed for the study of the atmospheric neutrino-induced upward-going muon flux in MACRO. It uses the Bartol neutrino flux [24], the Morfin and Tung parton density functions [25] for the calculation of the DIS νN cross sections, and the Lohmann et al. [22] muon energy loss for the propagation of induced muons through matter. The theoretical uncertainty on the expected event rate in MACRO for atmospheric neutrinos is ∼17%, mainly due to the uncertainty on the neutrino flux. Further details can be found in [26–28].

Fig. 5 (left) shows the distribution of the muon initial energy (i.e. muon energy when entering the detector) for the atmospheric neutrino simulated sample (dashed line) and for the AGN sample (solid line). The events surviving the analysis cuts $E_{\text{cut}} + D_{\text{cut}}$ are also shown (light shaded histogram for the atmospheric sample, dark shaded histogram for the AGN sample). The Fig. 5 (right) shows the distribution of the reconstructed energy released in the scintillator counters, with the same notation of the previous plot. The two distributions (atmospheric neutrino background and AGN signal) have been normalized to the same equivalent time of the AGN sample. A small number of background events survive the analysis cuts $E_{\text{cut}} + D_{\text{cut}}$. Because of the Monte Carlo generation statistics, the error bars (not shown) of the light shaded histograms, are at the level of 50% for each energy bin.

As a final remark, it should be noticed that the simulation of the atmospheric neutrino background does not take into account the isotropic contribution of neutrinos from semileptonic decays of charmed hadrons, usually called "prompt neutrinos". For neutrino energies above 10 TeV [30–32] this contribution should begin to dominate over the conventional pion and kaon decay induced neutrino flux. Actually, mainly due to the lack of precise information about high-energy
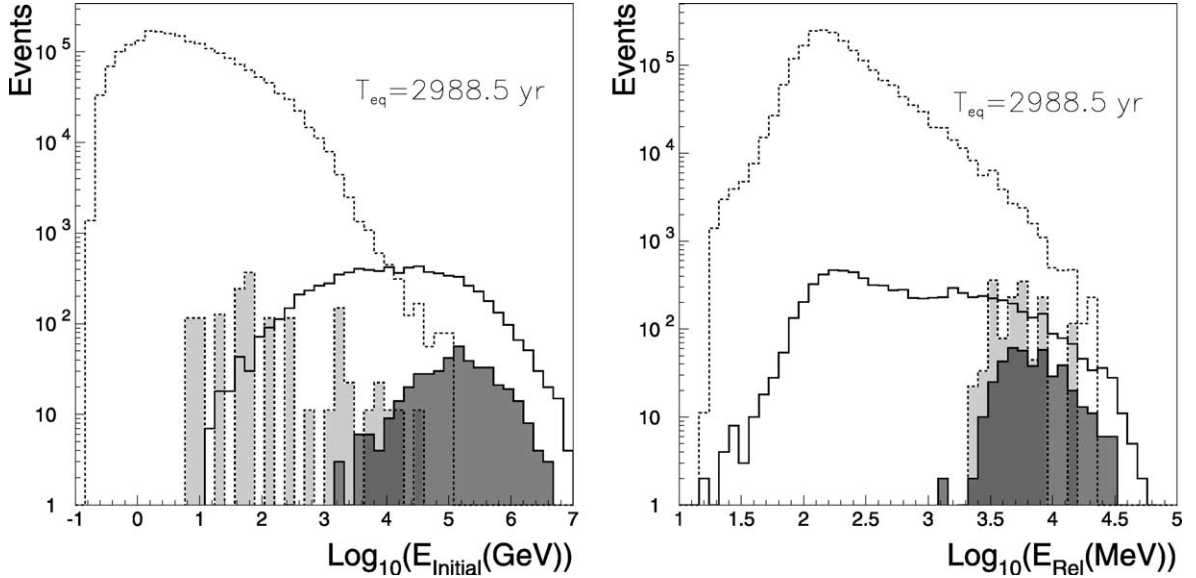
Fig. 5. (Left) Distribution of the muon initial energy for the AGN sample (—) and for the atmospheric neutrino background (- - -). The events surviving $E_{cut} + D_{cut}$ are shown as the light shaded histogram (atmospheric sample) and as the dark shaded histogram (AGN sample). (Right) Distribution of the reconstructed energy released in the scintillators, with exactly the same notation as for the plot in the left.

charm inclusive cross sections, the expected fluxes of prompt neutrinos, as well as the energy above which they start to dominate, fluctuate on a very wide range. Even by assuming one of the highest prompt neutrino flux prediction given in [32], the contribution to the signal has been estimated as few percent of the conventional atmospheric neutrino background (at least in the energy range in which this analysis is sensitive).

In Fig. 6 the contribution from prompt neutrinos, according to the maximum (PN_{max}) and the minimum (PN_{min}) predictions given in [32], are shown, together with the flux of conventional atmospheric neutrino and the diffuse fluxes of neutrinos from AGNs and GRBs according to some predictions.

5. Data analysis and results

The data used for this analysis were collected in the period from April 1994 to December 2000 (5.8 years, including efficiencies). After imposing the energy cut, E_{cut}, and the flight direction cut, D_{cut}, 97 real events survive.

Three events were rejected due to the action of a cut on the quality of the data. This quality cut (applied in all MACRO analyses which use the ERP TDCs) requires that the two TDCs, which have a different dynamic range, on each ERP channel must agree. This inefficiency, calculated from different analysis, affect 2% of the data sample [27,28].

As expected, a large contamination from multiple muons and near horizontal events is found. Those background events were rejected with the cut S_{cut}; after applying this cut, only two events survive. Fig. 7 shows the distribution of the quantity $1/\beta$ for one of the two selected event. The $1/\beta$ for the scintillator tracks fulfilling the conditions on geometrical length and on timing quality are shown as the shaded histogram.

An attempt to reconstruct the direction of both events has been performed by combining scintillator counters with streamer tubes tracking information. Because of the strong showering activity, the result is affected by a too high uncertainty for any directional astronomy study.

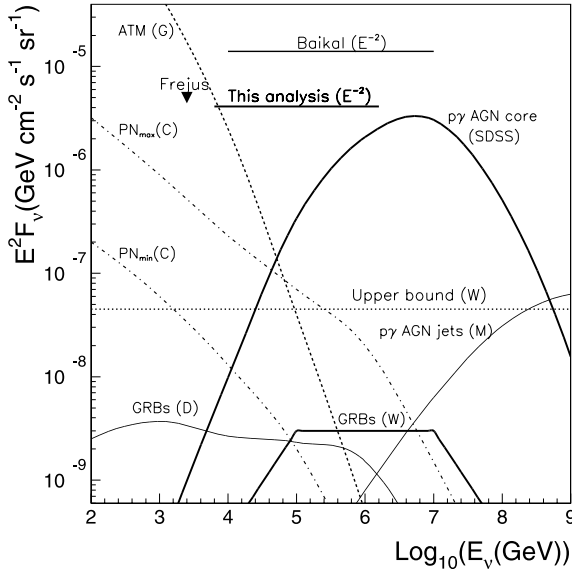The simulated AGN signal events have been processed with the same analysis chain as the real

Fig. 6. Diffuse fluxes of $\nu_\mu + \bar{\nu}_\mu$ from AGNs and GRBs according to many predictions. (SDSS) Stecker et al., 1991 [18]; (M) Mannheim, 1995 [34]; (W) Waxman and Bahcall, 1998 [35]; (D) De Paolis et al., 2001 [36]. The dashed curve refers to the angle average atmospheric neutrino flux; (G) Gaisser et al.,1995 [1]. The dash-dotted lines refer to the flux of prompt neutrinos according to the maximum (PN_{max}) and the minimum (PN_{min}) predictions given in [32]. The dotted line is the theoretical upper bound to neutrino fluxes from astrophysical sources as calculated in [35]. Some current published experimental upper limits are also shown. See Table 2 for references to the experiment results.

data; they are reduced by a factor (2%) which takes into account the above ERP inefficiency, not explicitly reproduced in the simulation of the detector response. 242/13305 simulated upward-going muons from diffuse AGNs survived all cuts. These events correspond to 0.54 for 5.8 years live time. For the atmospheric neutrino background, 1.1 events are expected in the same running period. The results are summarized in Table 1. The MACRO display of the two real events is shown in Fig. 8.

5.1. The upper limit

The data show no evidence of possible excess due to a diffuse neutrino flux from AGNs within the framework of the model [18]. Our result was used to set a muon flux upper limit F_μ^L which was calculated at 90% confidence level:
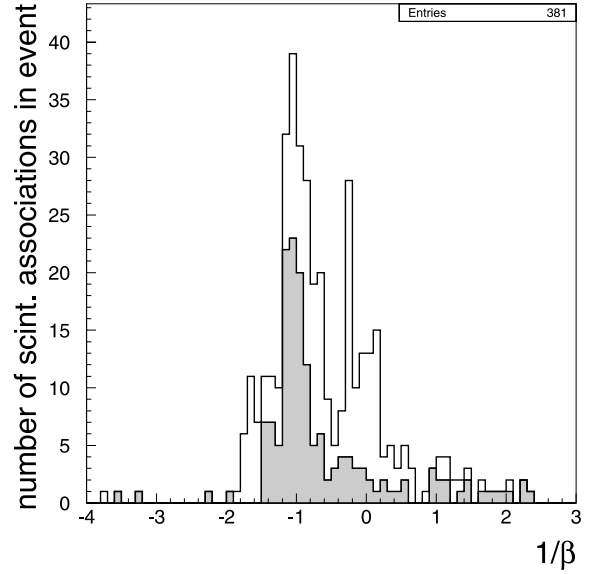

Fig. 7. $1/\beta$ distribution for one of the two events (Run 16399, Evt 2925) surviving all the analysis cuts. One entry corresponds to one scintillator track. The scintillator tracks fulfilling both the conditions on geometrical length and on timing quality are shown as the shaded histogram.

Table 1
Expected rate of events surviving all analysis cuts in 5.8 years of MACRO running

|	Rate of survived events in 5.8 years
Atmospheric (MC)	1.1 ± 0.5
AGN (MC)	0.54 ± 0.03
Data	2

Besides the number of events in the data, the expectation from the atmospheric background and the AGN neutrino flux (according to [18]) are shown. Only the statistical errors of the simulation were considered.

$$F_\mu^L = \frac{\text{upper limit (90\% c.l.)}}{\epsilon \times \int \text{Area}(\Omega)\, d\Omega \times T_l} \qquad (3)$$

The calculation of the numerator is based on the observation of two events when the expected background is 1.1 events, according to the recent approach of Feldman and Cousins [33]. ϵ is the fraction of simulated AGN events which survive the analysis cuts; Area(Ω) is the geometrical area seen by the diffuse flux as a function of the solid angle Ω (the integral extends to the lower Earth

RUN 16399   EVENT 2925   at 1:28:12.77   on 9/14/1998

	T	C	B	E	W	N	S
Number of scintillator boxes	7	6	10	2	7	0	0
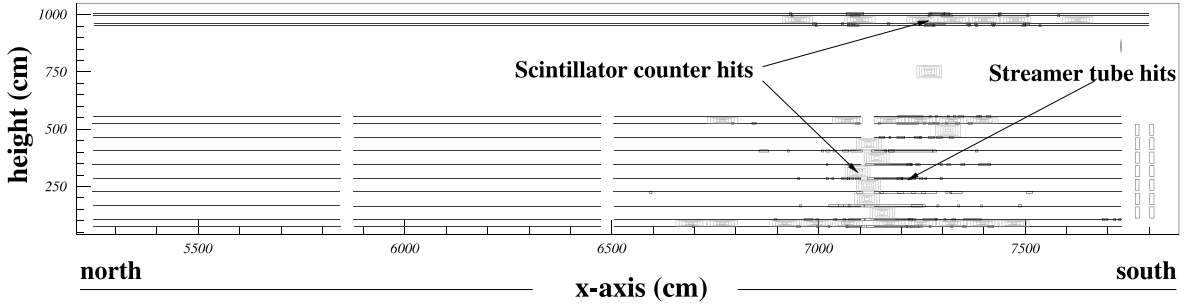
RUN 19574   EVENT 2198   at 10:33:47.90   on 5/24/2000

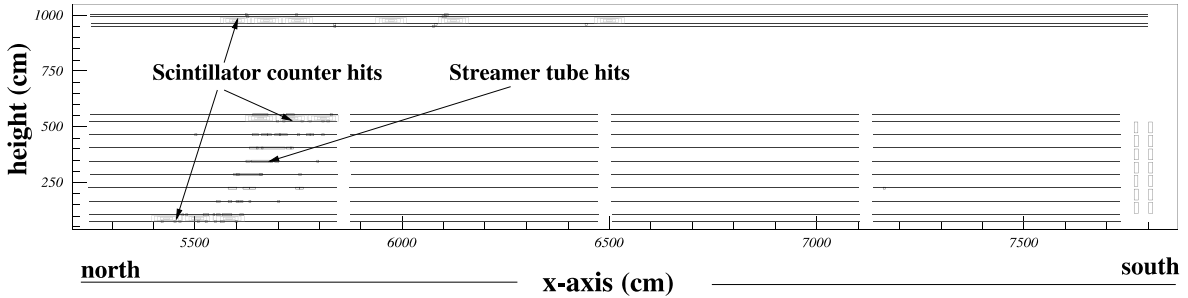|	T	C	B	E	W	N	S
Number of scintillator boxes	6	3	3	0	0	0	0

Fig. 8. Display of the two surviving events (longitudinal view) along the *x*-axis. The horizontal lines represent the 10 + 4 planes of horizontal streamer tube wires in the bottom and in the "Attico" parts of the detector. The wire hits are represented by black points. The gray boxes represent scintillator hits. Thirty-two scintillation counters overall fired in the first event which correspond to 381 scintillator tracks, whose $1/\beta$ values are shown in Fig. 5. Twelve counters fired in the second event. The location of fired scintillation counters is also given: T → Top, C → Central, B → Bottom, E → East, W → West, N → North, S → South, respectively.

hemisphere) and $T_l = 5.8$ years is the considered MACRO live time. With these values the muon flux upper limit becomes:

$$F_\mu^L(90\% \text{ c.l.}) = (1.7 \pm 0.2) \times 10^{-14} \text{ cm}^{-2} \text{ s}^{-1} \text{ sr}^{-1}$$

$$(4)$$

This limit can be finally converted into a (differential) neutrino flux upper limit. In order to compare our results with the upper limits given by other experiments, it is convenient to assume a power law spectrum with spectral index 2 for the initial neutrino flux. We have then weighted the number of surviving events with the ratio between this spectrum and the spectrum calculated by Stecker et al. With these hypotheses, the neutrino flux upper limit from this analysis is $E^2 F_\nu^L = (4.1 \pm 0.4) \times 10^{-6}$ GeV cm^{-2} s^{-1} sr^{-1}. Actually, this value must be considered carefully because it is affected by model assumptions (initial spectrum, neutrino cross sections and muon energy losses). Here, it has been estimated for comparison purposes.

Table 2
Neutrino flux upper limits (90% c.l.) from current experiments

	$E^2 F_\nu^{\mathrm{L}}$ (90% c.l.) (GeV cm^{-2} s^{-1} sr^{-1})	Neutrino energy range (GeV)
EAS-TOP [37]	2.0×10^{-3}	10^5–10^6
SPS-DUMAND [38]	6.0×10^{-4}	10^5–10^6
Baikal [2]	1.4×10^{-5}	10^4–10^7
Baikal (ν_e) [39]	1.3–1.9×10^{-6}	10^4–10^7
Frejus [40]	5.0×10^{-6}	$\sim 2.6 \times 10^3$
MACRO (this analysis)	$4.1 \pm 0.4 \times 10^{-6}$	10^4–10^6
AMANDA [41]	1.0×10^{-6}	10^3–10^6

The neutrino sensitivity range is shown in the last column.

Fig. 6 shows some theoretical predictions of neutrino fluxes from astrophysical sources (AGNs and GRBs) in comparison with upper limits obtained by current experiments. A list of them with references and energy range of sensitivity is given in Table 2.

6. Conclusions

We presented the results of a search for a diffuse neutrino flux from unresolved astrophysical sources by analyzing a sample of high-energy events collected by MACRO. We tested the detector response at high energy taking special care for the reliability of the scintillation counter response to high-energy particles. We used the reconstructed energy released in the scintillators to select a sample of high-energy events. Two high-energy upward-going candidates have been found in 5.8 years of effective running time. This number is compatible with the expected atmospheric neutrino background (1.1 events). The analyzed data have been used to set a muon and neutrino flux upper limit comparable with the results given by other experiments.

References

[1] T.K. Gaisser, F. Halzen, T. Stanev, Phys. Rep. 258 (1995) 173.

[2] BAIKAL Collaboration, V.A. Balkanov et al., Astropart. Phys. 14 (2000) 61.

[3] AMANDA Collaboration, E. Andres et al., Nature 410 (2001) 441.

[4] MACRO Collaboration, M. Ambrosio et al., Ap. J. 546 (2001) 1038.

[5] B. Szendy et al., Ap. J. 444 (1995) 415.

[6] Baksan Collaboration, M.M. Boliev et al., Proc. 24th Int. Cosmic Ray Conf. 1 (1995) 722.

[7] SuperKamiokande Collaboration, S. Matsuno et al., Proc. 27th Int. Cosmic Ray Conf. (2001).

[8] http://antares.in2p3.fr/;
E. Aslanides et al., ANTARES PROPOSAL: A deep sea telescope for high energy neutrinos, 1999, astro-ph/9907432.

[9] Available from <http://www.ssec.wisc.edu/a3ri/icecube/>.

[10] Available from <http://nemoweb.lns.infn.it/documentazione/proposal/>.

[11] Available from <http://www.nestor.org.gr/>.

[12] J.G. Leanerd, K. Mannheim, Annu. Rev. Nucl. Part. Sci. 50 (2000) 679.

[13] MACRO Collaboration, A. Corona, Proc. 24th Int. Cosmic Ray Conf. (1995).

[14] Geant Long Writeup W5013, CERN Program Library, 1994.

[15] MACRO Collaboration, S.P. Ahlen et al., Nucl. Instr. Meth. A 324 (1993) 337;
MACRO Collaboration, M. Ambrosio et al., Nucl. Instr. Meth. A 488 (2002) 663.

[16] S. Bottai, L. Perrone, Nucl. Instr. Meth. A 459 (2001) 319.

[17] MACRO Collaboration, M. Ambrosio et al., Astropart. Phys. 6 (1997) 113.

[18] F.W. Stecker, C. Done, M.H. Salamon, P. Sommers, Phys. Rev. Lett. 66 (1991) 2697, Erratum: 69 (1992) 2738.

[19] V.A. Naumov, L. Perrone, Astropart. Phys. 10 (1999) 239.

[20] H. Plothow-Besch, PDFLIB, Cern-ppe rep. 07.02, 1997.

[21] CTEQ Collaboration, H.L. Lai et al., Eur. Phys. J. C 12 (2000) 375.

[22] W. Lohmann, R. Kopp, R. Voss, CERN yellow report 03, 1985.

[23] R. Gandhi, C. Quigg, M. Hall Reno, I. Sarcevic, Phys. Rev. D 58 (1998) 093009.

[24] V. Agrawal, T.K. Gaisser, P. Lipari, T. Stanev, Phys. Rev. D 53 (1996) 1314.

[25] J.G. Morfin, W.K. Tung, Z. Phys. C 52 (1991) 13.

[26] Macro Collaboration, T. Montaruli, Proc. 27th Int. Cosmic Ray Conf. (2001);
Macro Collaboration, M. Spurio, Proc. 27th Int. Cosmic Ray Conf. (2001).

[27] Macro Collaboration, M. Ambrosio et al., Phys. Lett. B 434 (1998) 451.

[28] MACRO Collaboration, M. Ambrosio et al., Phys. Lett. B 478 (2000) 5.

[30] V.A. Naumov, T.S. Sinegovskaya, S.I. Sinegovsky, Nuovo Cimento A 111 (1998) 129 (see also hep-ph/9802410).

[31] P. Gondolo, G. Ingelman, M. Thunman, Astropart. Phys. 5 (1996) 309.

[32] C.G.S. Costa, Astropart. Phys. 16 (2001) 193.

[33] G.J. Feldman, R.D. Cousins, Phys. Rev. D 57 (1998) 3873.

[34] K. Mannheim, Astropart. Phys. 295 (1995).

[35] E. Waxman, J. Bahcall, Phys. Rev. D 59 (1998) 023002.

[36] F. De Paolis, G. Ingrosso, D. Orlando, L. Perrone, Astropart. Phys. 18 (2002) 249;
see also astro-ph/0107589.

[37] EAS-TOP Collaboration, M. Aglietta, Phys. Lett. B 333 (1994) 555.

[38] SPS-DUMAND Collaboration, J.W. Bolesta, Proc. 25th Int. Cosmic Ray Conf. 7 (1997) 29.

[39] Baikal Collaboration, V.A. Balkanov et al. Available from <astro-ph/0105269>.

[40] Frejus Collaboration, W. Rhode et al. Astropart. Phys. 4 (1996) 217.

[41] F. Halzen, presented to ph Neutrino Oscill. Work, 2000.